Available online at www.sciencedirect.com

SCIENCE DIRECT®

Cold Regions Science and Technology 39 (2004) 181–192

cold regions science and technology

www.elsevier.com/locate/coldregions

The rheology of snow in large chute flows

M.A. Kern[a,*], F. Tiefenbacher[a], J.N. McElwaine[b]

[a] WSL Eidgenössisches Institut für Schnee-und Lawinenforschung (SLF), Davos Dorf CH-7260, Switzerland
[b] Department of Applied Mathematics and Theoretical Physics, Cambridge University Wilberforce Road, Cambridge CB3 0WA, UK

Received 1 September 2003; accepted 24 March 2004

Abstract

The velocity profile and basal shear force were measured for snow flowing down a chute 34 m long and 2.5 m wide. The flows were approximately steady by the end of the chute where measurements were taken and the angle was 32°. Measurements of the basal shear stress confirm approximate dynamic balance. The velocity profile was measured using optoelectronic sensors and showed a large slip velocity at the base, a shear layer of around 50 mm and an overlying plug-like flow of about 350 mm. The velocity profile is compatible with both a Herschel–Bulkley rheological model, which combines a constant critical stress with a power law dependence on the mean shear rate, and a Cross model where the effective viscosity varies between two limits. Estimates of the Reynolds number suggest that the flow is not turbulent. The measurements are used to estimate the distribution of energy dissipation and to show that its concentration near the base may locally melt the snow, and thus serve as an explanation for icy melt surfaces observed at the base of flowing avalanche tracks.

Keywords: Avalanche dynamics; Channel flows; Snow rheology

1. Introduction

Despite decades of research, the constitutive behaviour of flowing snow is still not understood, though many (semi)empirical and theoretical attempts have been made to describe the flowing behaviour of avalanche-like flows (Dent and Lang, 1983; Dent, 1986, Norem et al., 1986, 1989; Hutter and Koch, 1991; Savage and Hutter, 1991; Koch et al., 1994; Louge, 1994; Hwang and Hutter, 1995; Bartelt et al., 1997). Without a verified constitutive relation of flowing snow, including boundary conditions, it is impossible to develop genuinely predictive avalanche models—that is dynamic models where the parameters can be related to measurements of the snow cover.

A common approach in modelling the dense layer of an avalanche is to depth average the continuum momentum balance equations with a specified non-Newtonian constitutive behaviour. These models are usually based on several assumptions that include the following:

(1) snow may be modelled as a continuum,
(2) snow may be considered as a simple fluid, that is the constitutive relation of the snow may be written as

$$\tau = \tau(\mathbf{D}), \tag{1}$$

as where τ is the deviatoric stress tensor and $\mathbf{D}$ is the deformation rate tensor: $D_{ij} = 1/2(\partial_j v_i + \partial_i v_j)$,

* Corresponding author. Tel.: +41-81-4170-159; Fax: +41-81-4170-110.
E-mail address: kern@slf.ch (M.A. Kern).

0165-232X/$ - see front matter © 2004 Elsevier B.V. All rights reserved.
doi:10.1016/j.coldregions.2004.03.006

(3) snow is incompressible,
(4) the flow is laminar,
(5) vertical velocities can be neglected.

The depth averaged downslope momentum equation then takes the form

$$\frac{\partial \bar{v}}{\partial t} + \frac{1}{2}\frac{\partial \overline{v^2}}{\partial x} = \text{source terms}, \quad (2)$$

where $\bar{v} = 1/H \int_0^H v dy$ is the average downslope velocity and $\overline{v^2} = 1/H \int_0^H v^2 dy$.

Most experimental data (Gubler, 1986; Nishimura and Maeno, 1986; Nishimura, 1990; Nishimura and Ito, 1997; Dent et al., 1997) suggests that $\overline{v^2} \approx \bar{v}^2$, so that Eq. (2) can be approximated well by

$$\frac{\partial \bar{v}}{\partial t} + \bar{v}\frac{\partial \bar{v}}{\partial x} = \text{source terms}, \quad (3)$$

which has the same left-hand side as a flow with uniform velocity profile. This appears to suggest that for snow flows the internal constitutive behaviour is not particularly important. However, the source terms on the right-hand side include boundary terms from the depth integration that depend sensitively on the constitutive behaviour. Without an accurate understanding of the constitutive behaviour, they cannot be related to snow properties and flow variables, but instead must be fitted to a particular experiment or avalanche. Only after understanding the constitutive behaviour can Eq. (2) even be justified. Of course, also additional variables, such as granular temperature (Jenkins and Mancini, 1987), may be necessary for closure.

A chute may be used as a rheometer for fluids in variety of ways. For example, by computing the flow curve for steady simple shear flow from the discharge curve (Ancey et al., 1996). In this work, we infer properties of the constitutive behaviour of flowing snow from velocity profile measurements. A rheological model can then be tested by comparing its predicted velocity profile with the measurements if its parameters and boundary conditions are specified. However, if the parameters are unknown and must be fitted to the experimental data, a variety of experiments at different flow depths, angles and boundary surfaces should be performed. The great difficulty of performing experiments with snow is that the snow can vary from experiment to experiment. The large size of the chute also means that only one or two experiments can be performed per day if there are appropriate weather and snow conditions. Because of these difficulties, we present data from only a few experiments and show that they are consistent with two different rheological models.

2. Experimental setup

2.1. Chute design

Flows of snow were generated on a 34 m long and 2.5 m wide chute which is located near the building of the Swiss Federal Institute of Snow and Avalanche Research on the Weissfluhjoch, near Davos, Switzerland at 2670 m a.s.l. A schematic of the chute is given in Fig. 1. The chute consists of a 20-m-long section, whose inclination can be varied between 35° and 45°. For the results presented in this paper, the angle was 45°. The next section is the runout section where the angle changes in steps of 4.2, 6.05 and 3.5 m from 32° to 25° and then to 8° inclination. The upper half of the inclinable part of the chute can be filled with snow, which is released by opening the gate 10 m from the top. If the bottom of the chute is smooth, then a plug-like flow forms sliding on the metal surface. To create a basal shear layer of finite thickness, the base was roughened by rubber bars with the dimensions $24 \times 60 \times 600$ mm (height, width, length).These rubber bars are connected together with a streamwise

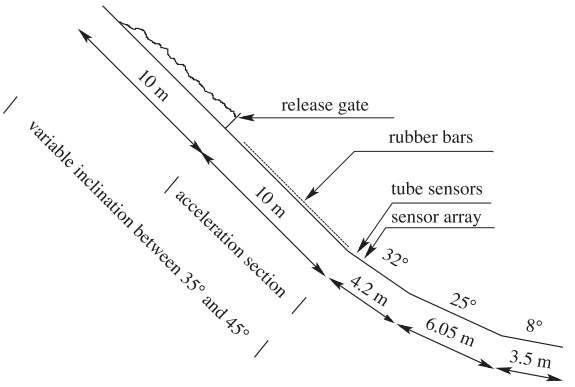

Fig. 1. Side view of the Weissfluhjoch snow chute. The downstream distance between tube and array sensors is about 0.5 m.

spacing of 25 mm to form a mat with the dimensions 2×8 m where the upper boundary of the mat is placed about 2 m downslope of the release gate. In the experiments with rubber mats, the flowing snow experiences considerable shear in an about 5–10-cm-thick layer near the bottom.

2.2. Basal shear stress measurement

The downstream basal shear stress exerted by the flowing snow on the mats was measured by piezo force gauges, which are connected to the rubber mats by wire ropes. For a more detailed discussion, see Tiefenbacher and Kern (2004).

2.3. Velocity profile measurement

To measure the flow velocity, optoelectronic sensors were placed on the sidewall and in the middle of the 32° angle section of the chute at the positions indicated in Fig. 1. The measurement principle is based on the cross correlation of signals of two reflectivity sensors with a downstream spacing and has, with some technical sophistication, been adopted from Nishimura et al. (1993) and Dent et al. (1997). The profile line at the sidewall is formed by six tube sensors, which each consist of two reflectivity sensors with a downstream displacement of 12 mm in a metal tube and whose baselines are situated, respectively, 0, 39, 68, 101, 132 and 186 mm above the rubber mat surface. At the centreline, 25 reflectivity sensors are placed behind a half wedge which slices the flow in such a way that the flow passing the sensors can be regarded as to be nearly undisturbed. These 25 sensors are placed in five rows of each five sensors with a vertical spacing of 11 mm. The downstream spacing of the five sensors placed in a row is about 4 mm. Within a 50-mm-thick basal shear layer of the experimental chute flows, this configuration provides a vertical spatial resolution of the velocity profile of 11 mm with a high measurement accuracy, for the velocity can be determined by correlation of the signals of each of the 10 possible combinations of two reflectivity sensors per row. The reflectivity signals of the sensors are captured with a sampling frequency of 40 kHz at 16 bits by an A/D converter card and are stored in a PC, where they are further processed by a cross correlation analysis. For a thorough description of the technical details of the chute, the measurement devices and the data processing procedure, refer to Tiefenbacher and Kern (2004). Alternatively, more sophisticated methods of velocity data analysis are discussed in McElwaine and Tiefenbacher (2003).

3. Measurement results

In this section, we briefly describe the experimental observations which will be analysed in the next section.

3.1. General flow behaviour

The flow on the initial rough acceleration section of the chute has a typical flow height of about 0.4 m and it exhibits an avalanche-like head–tail structure with an approximately 8-m-long section of constant flow height in the middle of the flow. At the front, the flow height is about 20% higher than the middle section of the flow. Analysis of video recordings shows that the front velocity reaches terminal velocity after about 8 m (Fig. 2), that is before it reaches the velocity sensors. Thus, as a first approximation, we assume that the flow is steady at the velocity sensor position so that the mean downslope velocity is constant within the flow and depends only on depth.

To some extent, the time series of the basal shear stress resembles the visually observed head and tail structure, but it is also influenced by other effects such as chute vibrations. However, during the time interval, where the entire rubber mat was covered by flowing snow, an approximately steady mean basal shear stress of $\tau_R = 794 \pm 231$ kPa was measured (Tiefenbacher and Kern, 2004).

3.2. Velocity profiles

Velocity profiles have been measured by the line of tube sensors and by the sensor array, which was placed about 0.45 m downstream of the tube sensors at the chute centreline. Four measurements of the velocity profiles have been performed. The velocity profiles obtained by the tube sensors and by the array sensors are shown in Figs. 3 and 4. Due to technical problems,

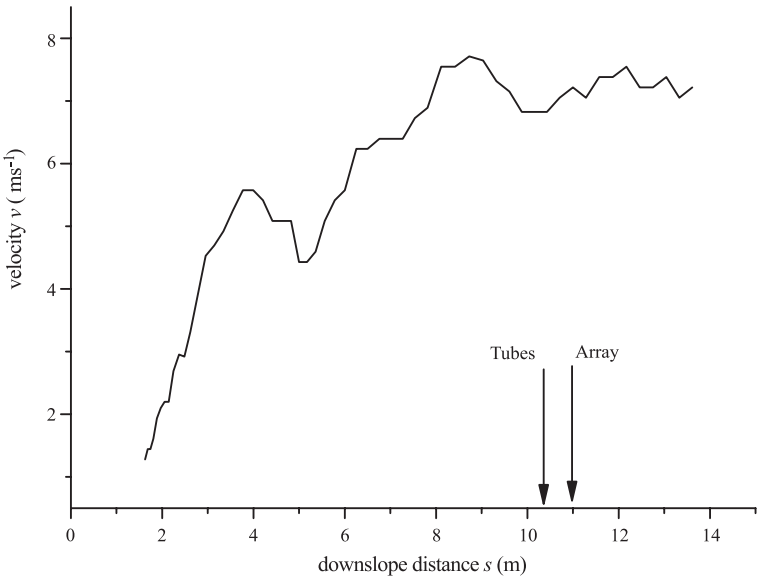

Fig. 2. Front velocity of the chute flow along the chute. The downslope position s is measured from the release gate.

only one velocity measurement could be performed in parallel with the basal shear stress measurement. For this reason, the following analysis is done with the data of this experiment, which was performed on May 15, 2002. As these data only slightly differ from the mean of the three experiments performed with wet snow, using the May 15 data is a reasonable approximation, as will be shown below.

The combined tube and array data of the May 15 experiment described in Section 2.3 is shown in Fig. 5. The sidewall velocities are 0.5 m s^{-1} slower than the velocities obtained by the sensor array at comparable heights. This effect is presumably due to sidewall friction. Accordingly, in Fig. 5, the tube sensor profile was shifted by 0.5 m s^{-1} which results in a velocity

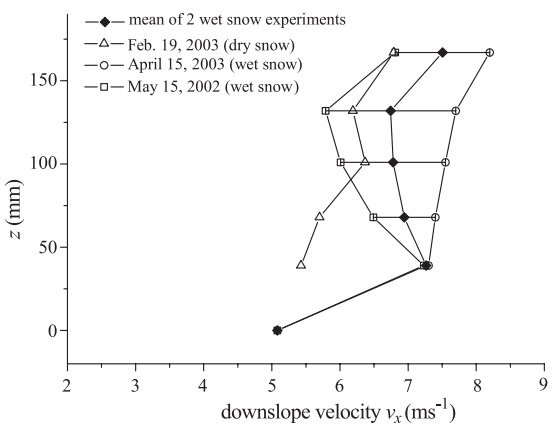

Fig. 3. Profiles of the downstream velocity obtained by the sidewall tube sensors.

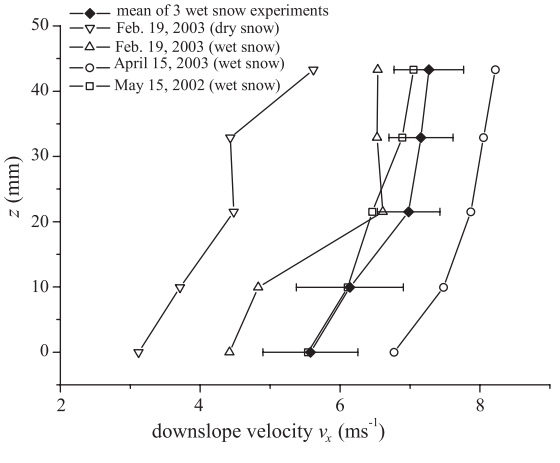

Fig. 4. Profiles of the downstream velocity obtained by the array sensor in the chute centreline.

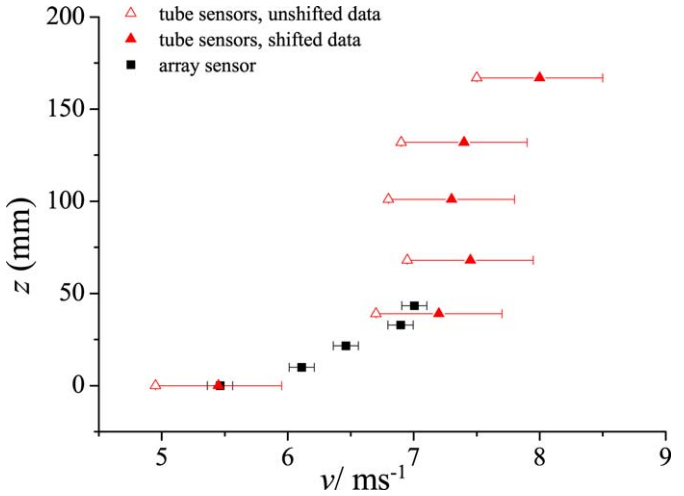

Fig. 5. Experimentally obtained velocity profile of the chute flow, which exhibits a shear layer with overburden plug-like flow layer. Squares: measurement results of the high-resolution sensor array, triangles: velocities obtained from tube sensors, shifted by 0.5 m s^{-1}.

profile which can be assumed to approximately resemble the flow state at the chute centreline.

The lowest 50 mm of velocity profile, as resolved by the array sensor, show slip of about 5.5 m s^{-1} and considerable shear of about 43 s^{-1}, while the shear in the overlaying 125 mm layer, as it is captured by the tube sensor line, is of the order of 6 s^{-1}. This may be interpreted as a hint to the general profile structure which is characterised by a high shear bottom layer and an overburden plug-like flow layer as shown in Fig. 6.

4. Analysis

As the stresses within the flowing snow are not experimentally accessible, we assume them to be

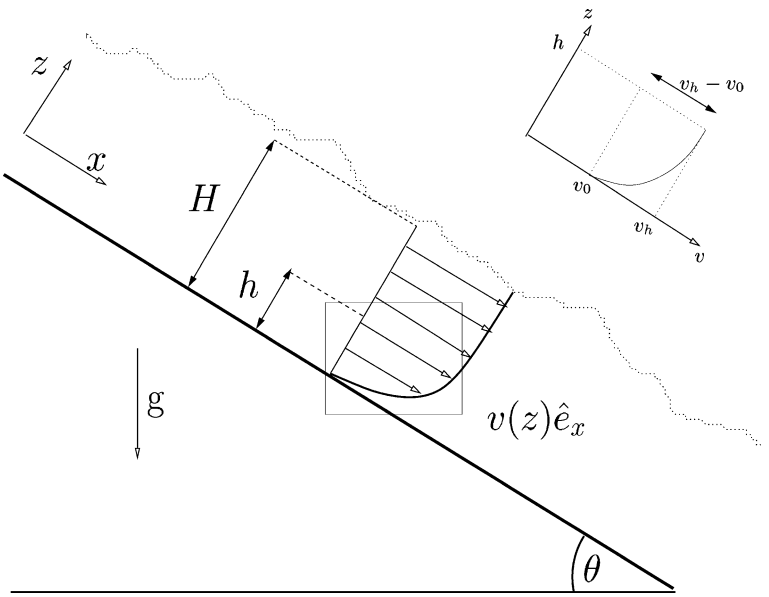

Fig. 6. Principle sketch of velocity profile.

determined by the averaged x-momentum equation for a steady shear flow with constant depth which reads

$$\frac{d\tau}{dz} + g\rho\sin\theta = 0, \qquad \mathbf{v} = v(z)\hat{e}_x, \tag{4}$$

where the mean density ρ of the flow is assumed to be constant. The mean stress $\tau = \tau_{xz}$ contains both viscous effects and averaging effects that result in Reynolds stresses. The averaging can be thought of as averaging in time or in space across and down the slope. The boundary conditions is that there are no surface tractions so that $\tau(H) = 0$, where H is the height of the flow. The solution of Eq. (4) is

$$\tau(z) = g\rho(H - z)\sin\theta. \tag{5}$$

That is the stress increases linearly with depth and the shear stress $\tau(0)$ on the basal surface is $\tau(0) = g\rho H\sin\theta_m$, where $\theta_m = 45°$ is the slope angle of the inclined part of the chute with the rubber mats. Using the values in Table 1, this is 1110 ± 196 Pa, which should be equal to the measured stress on the mats $\tau_R = 794 \pm 231$ Pa. This is a reasonable agreement as the error ranges overlap and one would also expect friction between the rubber mats and the bottom of the chute to reduce the measured shear stress.

4.1. Constitutive relations

The following analysis shows how the constitutive behaviour of flowing snow can be examined using a chute as a rheometer. However, the data in this paper is not sufficient to discriminate between different rheological models, but we show that it is consistent with the Herschel–Bulkley model and the Cross model (Barnes et al., 1989).

Table 1
Principal measurements and derived quantities

Variable	Value	Description
H	0.400 ± 0.050 (m)	Total flow depth
h	0.044 ± 0.006 (m)	Depth of the shear layer
ρ	400 ± 50 (kg m^{-3})	Flowing snow density
$\bar{v}$	7.19 ± 0.2 (m s^{-1})	Mean velocity at sensor position
v_0	5.46 ± 0.2 (m s^{-1})	Slip velocity
v_h	7.05 ± 0.2 (m s^{-1})	Velocity at upper boundary of shear layer
τ_R	794 ± 231 (Pa)	Stress on basal surface
θ	32°	Chute inclination at velocity sensor position
$\dot{\gamma}(0)$	69 s^{-1}	Basal shear rate

4.1.1. Herschel–Bulkley

Since for times less than a few hours snow can behave like a solid, a natural choice of a rheological model is Bingham (Oldroyd, 1947)—one of the simplest rheological models that includes both solid-like and fluid-like behaviour. Visco-plastic models have frequently been used as a description for the constitutive behaviour of flowing snow (Dent and Lang, 1983). However, we will show that our data rules out a Bingham model but is compatible with a generalisation—the Herschel–Bulkley model. Such a model recently was proposed to be included in future flowing avalanche models (Issler, 2003). We assume in this subsection that there is a shear layer of $h = 43$ mm underneath a plug-flow extending to the surface $H = 400$ mm. The yield stress is therefore $\tau_c = (H - h)g\rho\sin\theta = 740 \pm 100$ Pa.

In the Herschel–Bulkley model, the stress is given by

$$\tau \begin{cases} \leq \tau_c & \frac{dv}{dz} = 0 \\ = \tau_c + K\left(\frac{dv}{dz}\right)^{\alpha} & \frac{dv}{dz} \geq 0. \end{cases}, \tag{6}$$

where $\alpha \geq 1$. If we assume that there is a plug flow between h and H then Eq. (5) shows that $\tau_c = (H - h)g\rho\sin\theta$. For this section, we will assume a known slip velocity for the lower boundary condition, but this will be discussed in more detail in Section 5. Eqs. (5) and (6) can then be solved to give the velocity profile

$$v(z) = \begin{cases} v_h & h \leq z \leq H \\ v_h + (v_0 - v_h)\left(1 - \frac{z}{h}\right)^{\frac{1+\alpha}{\alpha}} & 0 \leq z \leq h \end{cases}, \tag{7}$$

where $v_h = v_0 + h\frac{\alpha}{1+\alpha}\left(\frac{h\rho g\sin\theta}{K}\right)^{1/\alpha}$ is the velocity at $z = h$ and v_0 is the velocity at $z = 0$. The units of the parameter K are of mixed power but we reparameterise the rheological model by defining the stress for non-zero shear as $\tau_c\left[1 + \left(t_c\frac{dv}{dz}\right)^{\alpha}\right]$, where t_c now has units of time.

The results of fitting this model to the data are shown in Fig. 7 and the parameter values are shown in Table 2. As well as the best values (least mean squares of velocity), minimum and maximum values for the exponent α are given so that the data is fitted to an accuracy of 0.12 m^{-1}. This value is slightly larger than the measurement errors but the data can then also be fitted by the degenerate case $\alpha=\infty$ corresponding to a linear velocity profile in the shear layer.

These results are similar to the velocity profile obtained by Norem et al. (1986, 1989) who derived it from general constitutive equations for cohesive granular material, where the shear stress was assumed to be proportional to the square of the shear rate, that is $\alpha=2$. One would also expect an $\alpha=2$ dependence if the shear rate dependent contribution to the stress was caused by Reynolds stresses. This agrees perfectly with our best fit value, but since the spread of values compatible with data is so large no definite conclusions should be drawn. The data is sufficient however to rule out a Bingham $\alpha=1$ rheology.

4.1.2. The Cross model

The Cross model is a generic rheological model where the effective viscosity varies between two limits with the shear rate. We consider a simplified Cross model with exponent one. The kinematic viscosity is defined by

$$\mu=\frac{\mu_0+\mu_1 k_c\dot{\gamma}}{1+k_c\dot{\gamma}}, \tag{8}$$

and the stress by $\tau=\rho\mu\dot{\gamma}$, where $\dot{\gamma}=dv/dz$. That is the viscosity varies smoothly between μ_0 for zero shear to μ_1 in the limit as $\dot{\gamma}\to\infty$ and k_c is a time scale that determines the range of shear that the transition occurs over. Solving this equation with a zero shear upper boundary condition and unspecified lower boundary has the solution

$$v=C+\frac{z'}{k_c}-\frac{g}{4\mu_1}\times\left[z'^2+z'\sqrt{a^2+z'^2}+a^2\sinh^{-1}\left(\frac{z'}{a}\right)\right], \tag{9}$$

where C is a constant that depends on the slip velocity, $\alpha=2\sqrt{\mu_1\mu_0-\mu_1^2}/(gk_c)$ and $z'=H+(2\mu_1-\mu_0)/(gk_c)-z$.

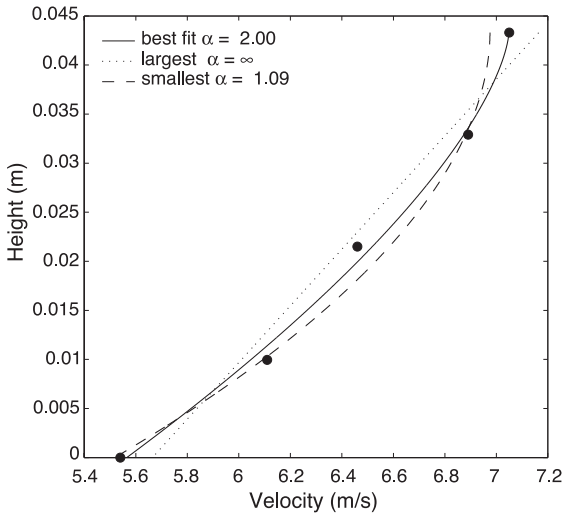

Fig. 7. Fit to the Herschel–Bulkley model of the shear layer velocity profile.

Table 2
Fit parameters for Herschel–Bulkley model (two significant figure)

Parameter	α	K (mixed)	t_c (s)
Best fit	2.0	0.033	0.0014
Smallest α	1.1	0.96	0.0017
Largest α	∞	–	0.0013

The minimum and maximum values of α that fitted the data to within 0.12 m^{-1} as well as the least mean squares fit.

The good agreement between the measured data (Fig. 5) and the Cross model is seen in Fig. 8 and the parameters are given in Table 3. The parameters are calculated using least mean squares error and the residual was 0.15 m s^{-1}. A hundred random samples were then generated by adding zero mean gaussian noise with this standard deviation and the parameters recalculated. The interquartile range of the parameter estimates is shown in Table 3. The true uncertainties are probably lower, particularly for the viscosity in the shear layer μ_0 where the measurements are more accurate.

4.2. Comparison with previous work

Early work on snow in fluidised beds (Maeno and Nishimura, 1979; Maeno et al., 1980) suggested kinematic viscosities of order 0.001 m^2 s^{-1}. In our

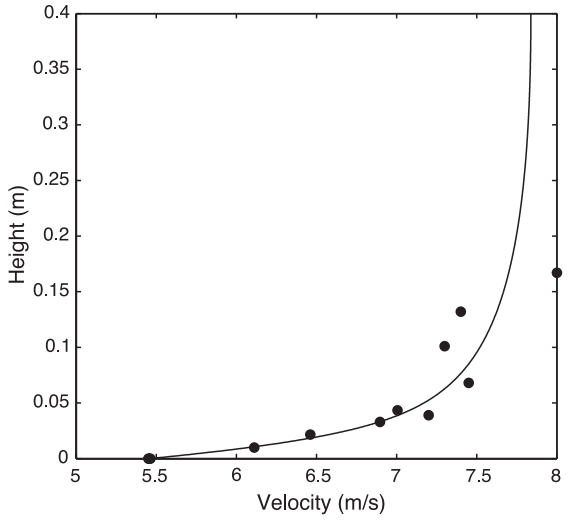

Fig. 8. Fit to the Cross model of the complete velocity profile.

experiments, the snow is not fluidised so one would expect higher values which is indeed the case. Interestingly, the Cross model predicts that at very high shear the kinematic viscosity will decrease to around 0.0027 $m^2\ s^{-1}$, which is of the same order of magnitude as Maeno's results. Dent and Lang (1982) performed experiments with very similar results (similar flow depths, velocities and shear layer thickness), but their measurements in the shear layer were less accurate and more widely spaced. They concluded that the data was well explained by a no-slip lower boundary condition with a Bingham rheology with a yield stress of $\tau_c = 540$ Pa for snow of density $\rho = 250–300$ kg m^{-3} so that $\tau_c/\rho = 1.8–2.2$ m s^{-2}. This is in excellent agreement with our value of $\tau_c/\rho = 1.9$ m s^{-2}. Dent and Lang (1982) estimated the kinematic viscosity as 0.004 m s^{-1} which is rather low compared to our measurements. The Cross model fit implies a shear rate of 69 s^{-1} at the base and an effective kinematic viscosity of 0.03 $m^2\ s^{-1}$—nearly 10 times larger. The explanation, however, is that because they assumed a no-slip boundary condition their estimate of the shear rate was much higher leading to lower estimates of the kinematic viscosity.

4.3. Shear layer Reynolds number

The Reynolds number can be used to estimate if a flow is likely to be turbulent or laminar. For Newtonian fluids, it is defined as $Re = \rho v L/\eta$, where η is the viscosity and L is a length scale. For non-Newtonian fluids, the situation is more complicated as there is no constant viscosity, but instead a collection of parameters that determine the stress. A common approach is to define the effective viscosity $\eta_e = \tau/\dot{\gamma}$ (Metzner and Reed, 1955). This is straightforward to apply to pipe and channel flows, where the stress and shear rate are taken as the wall values and the mean velocity is used. In this case, transition to turbulence occurs for Reynolds numbers of around 2000 (Mannheimer, 1991). However, Herschel–Bulkley rheology is usually used with a no-slip boundary condition. In our flows, there is a very large slip velocity so the shear rate is discontinuous at the boundary. The value at the boundary is infinite (implying zero viscosity), but if we use the limiting value of the shear rate from above we will overestimate the viscosity since the shear rate will be low. Instead we take the shear rate across the whole shear layer $v(h)/h$ and the largest length scale H. The mean velocity is very close to $v(h)$ so considering the Reynolds number for this layer we get

$$Re = \frac{\rho H v(h)}{\tau(0)/[v(h)/h]} = \frac{\rho H v(h)^2}{\rho g h H \sin\theta} = \frac{v(h)^2}{gh\sin\theta} \approx 220. \tag{10}$$

Note that this estimate is the square of the Froude number for the shear layer. It assumes that the flow is laminar, that is all the stresses are viscous in nature, which is consistent because Re is well below the threshold of 2000. Alternatively, we could assume a purely plastic constitutive behaviour so that the stresses above the critical stress are Reynolds stresses. The estimated Reynolds number would then be larger by a factor of $1 - h/H$, which is not significant.

Table 3
Fit parameters for the Cross model

Parameter	Units	Best fit	Interquartile range
k_c	s	1.10	0.71–1.17
μ_0	$m^2\ s^{-1}$	2.1	1.4–2.2
μ_1	$m^2\ s^{-1}$	0.0027	0.0010–0.0032
ν_0	kg $m^{-1}\ s^{-1}$	800	600–900
ν_1	kg $m^{-1}\ s^{-1}$	1.07	0.40–1.29

The dynamic viscosities $\nu_i = \rho\mu_i$ are also given for convenience.

This calculation is only a rough estimate of the Reynolds number, but never the less it is so far below the threshold, that it is a safe conclusion that laminar flow is stable with similar rheologies. This suggests four possibilities.

(1) One is that the flow is essentially laminar and the constitutive relation is entirely viscous and Reynolds stresses are small. This however seems unlikely as the flow of snow down a smooth channel without a rough bottom results in a much thinner shear layer of only a few millimeters.
(2) Another possibility is that the flow is only quasi-steady. That is the vertical velocities induced by the matting play an important part in the structure of the shear layer, but are not self-supporting. Thus we would expect the shear layer to gradually become thinner in a very long chute as the vertical motions die away and the flow to degenerate to the same plug-like steady state that would have been reached if an entirely smooth chute had been used.
(3) The third possibility is that there are stresses generated by the granular temperature which is related to the covariance matrix of the particle's velocities.
(4) The final possibility is that our estimate of the Reynolds number is inaccurate. If the yield stress is due to cohesion between snow particles, one might expect the viscous stress to fall very rapidly with shear rate before increasing, the balancing stress being due to Reynolds stresses. The minimum value of the effective viscosity $\tau(\dot{\gamma})/\gamma$ would then determine the Reynolds number.

4.4. Energy dissipation

We can use the velocity measurements to estimate the energy dissipation in the flow. As a direct consequence of the momentum conservation equation, gravitational work on the flowing snow has to be balanced by the energy dissipation at the sliding surface and in the shear layer. Consequently, checking the energy balance does not provide a new insight into the flow behaviour. It might, however, be of some practical interest to discuss the estimated values of energy dissipation with respect to observations at real avalanches. The bases of avalanche tracks frequently exhibit an icy surface, which is suspected to be due to the melting of snow at the basal sliding surface. Fig. 9 shows an example of such an avalanche track.

In what follows, we demonstrate that our experimental results are compatible with the assumption of basal melting due to energy dissipation at the basal layer of the flowing avalanche. To do so, we start with the local energy dissipation w_s in the flow which is the rate of work done by the stress on fluid particles: $w_s = \tau\,(\mathrm{d}v)/(\mathrm{d}z)$. Integrating w_s over the depth of the flow and using Eq. (5) to eliminate $\tau(z)$, we may write down the total internal energy dissipation $W_s = \int_0^H w_s \mathrm{d}z$.

$$W_s = \int_0^H \tau \frac{\mathrm{d}v}{\mathrm{d}z}\mathrm{d}z = [\tau v]_0^H - \int_0^H v\frac{\mathrm{d}\tau}{\mathrm{d}z}\mathrm{d}z = \rho g H \sin\theta(\bar{v} - v_0), \tag{11}$$

where $\bar{v}=1/H\int_0^H v\ \mathrm{d}z$ is the mean velocity.

Eq. (11) shows that the dissipation in the flow is proportional to the excess of the mean velocity over the slip velocity. Thus, for a complete plug flow where these are equal, all the energy is dissipated in the basal layer. The other extreme is when there is a no-slip boundary condition, so that $v_0 = 0$ and then all the energy is dissipated in the flow. The right-hand side of Eq. (11) can be interpreted as the difference between the rate of gravitational working $W_g = gH\rho\sin\theta\bar{v}$ and

Fig. 9. Base of a flowing avalanche track with an icy surface. Vallee de la Sionne, Valais, Switzerland, photograph: Andi Felber, SLF.

the rate of energy dissipation on the basal surface, which is $W_b = \tau(0)v_0 = gH\rho\sin\theta v_0 = v_0\tau_R$. So we may write for a steady flow

$$W_s + W_b = W_g. \tag{12}$$

Using the values in Table 1 we calculate

$$W_b = v_0\tau_R = (4335 \pm 1271)\mathrm{Wm}^{-2},$$

$$W_s = \int_0^H \tau \frac{\mathrm{d}v}{\mathrm{d}z}\mathrm{d}z = (1438 \pm 1519)\mathrm{Wm}^{-2},$$

$$W_g = gH\rho\sin\theta\bar{v} = (5980 \pm 1070)\mathrm{Wm}^{-2},$$

where W_s has been calculated from the fitted velocity profile in the shear layer (Eq. (7)) for the Herschel–Bulkley model.

Given the accuracy of our results, energy dissipation within the plug-like layer appears unimportant. Most of the energy is dissipated on the basal surface with the remaining fifth within the shear layer. However, the inaccuracy of the results indicated by the error ranges would, in principle, also allow for a considerable energy dissipation due to particle collision processes in the low shear plug-like layer.

To estimate over what distance an avalanche must travel before melting can occur, we compute the temperature change rate and the melting rate for the shear layer of the experimental flow. The latent heat of fusion for ice is $s = 334$ kJ kg^{-1}, so that if all the dissipated energy went into melting ice the rate would be 17.3 g s^{-1} m^{-2}, but if the energy dissipation were evenly distributed the snow would have to fall a vertical distance of $s/g = 34$ km to melt completely. Thus a very uneven distribution is necessary for melting to occur in avalanches. In addition before snow melting can occur, the temperature of the snow at the sliding surface has to be increased to 0 °C.

To estimate the time needed for this temperature increase, we solve the 1D heat conduction equation

$$\frac{\partial T}{\partial t} = \frac{k}{\rho c}\frac{\partial^2 T}{\partial z^2}, \tag{13}$$

where $c = 4.19$ kJ kg^{-1} K^{-1} is the specific heat capacity of ice and k the thermal conductivity. We consider a snow block at initial temperature

$$T(t = 0, z = 0) = T_0, \tag{14}$$

which is heated by the energy dissipation at the base of the flow ($z = 0$). That is, the boundary condition for $z = 0$ is a constant flux of heat

$$\frac{1}{2}W_s = \begin{cases} k\left.\dfrac{\partial T}{\partial z}\right|_{z=+0} \\ -k\left.\dfrac{\partial T}{\partial z}\right|_{z=-0} \end{cases}, \tag{15}$$

where k is the heat conduction coefficient of snow. The factor of two is because half the heat diffuses upwards into the flowing snow and half down into the snow pack. The solution of Eq. (13) with respect to Eqs. (14) and (15) reads

$$T(z,t) = T_0 - \frac{W_s z}{2k}\mathrm{erfc}\left(\frac{z}{2\sqrt{\kappa t}}\right) + \frac{W_s}{\rho c}\sqrt{\frac{t}{\pi\kappa}} \times \exp\left(-\frac{z^2}{4\kappa t}\right), \tag{16}$$

where $\kappa = k/\rho c$. The time evolution of the temperature at the basal surface $z = 0$ is

$$T(z = 0, t) = T_0 + \frac{W_s}{\rho c}\sqrt{\frac{t}{\pi\kappa}}. \tag{17}$$

For $T_0 = -10$ °C, and $k \approx 1$ W m^{-1} K^{-1}, we find the time $t_{-10\,^\circ\mathrm{C}}$ necessary to increase the basal snow temperature up to the melting point to be $t_{-10\,^\circ\mathrm{C}} = 64$ s (equivalent to 400 m). This means that the chute flows which we created within our experiments are not long enough to start basal melting if the snow is −10 °C cold. As the warming time to the melting point is quadratic in the temperature difference to 0 °C, for "warmer" snow melting would be possible on the chute even for the short travelling time of the chute flow. Real avalanches can of course flow much further than in our experiments. The flowing avalanche leading to the icy surface shown in Fig. 9 was observed to travel down the track for more than 1 min. Assuming the same basal energy dissipation as for the chute flow (which is most probably a lower bound estimation), we would expect approximately 1 kg m^{-2} of molten snow half in the stationary snow pack and half in the avalanche. This raw estimation is compatible with the observation of an ice crust of some millimeter thickness in the avalanche track described above.

5. Boundary conditions

Though this paper has focused on the internal dynamics of the flow, another important question is the correct basal boundary condition. This determines the overall speed of the flows and the runout distance of an avalanche. Even with the extremely roughened base, the slip velocity was 5.5 m s^{-1} as compared to an internal velocity difference of only 1.5 m s^{-1}. What determines this slip velocity? The data presented in this paper is not adequate to answer this question. A Coulomb friction type force would suggest a friction angle identical to the slope angle, but without any velocity dependence steady state flows will not result. Assuming a local theory, the boundary condition must be some relation between $u(0)$, $\dot{\gamma}$, ρ, and $\rho gH\cos\theta$ (we neglect the possibility of dependence on higher derivatives). The simplest dependence would be $u(0) \propto \sqrt{gH\cos\theta}$. This is a Froude number type condition and our data suggests that $Fr = u(0)/\sqrt{gH\cos\theta} \approx 3.0 - 3.8$. More complicated relations involve introducing additional dimensional parameters. A boundary condition often used in fluid dynamics is $u(0) - L\dot{\gamma} = 0$, where L is the slip depth $\approx$ 0.08–0.16 m. Both of these relations would imply that a flow with a thicker shear layer would have a higher mean velocity than an otherwise identical flow with a thinner shear layer, if we can assume that the thickness of the shear layer adjusts to the boundary conditions over a slow time scale. These possibilities could be distinguished by performing experiments of different depths with and without mats.

6. Conclusions and outlook

In this contribution, we presented some experimental results about the velocity structure and about the basal friction forces of sheared flow of snow on a rough surface. The observed chute flows of snow exhibit a shear layer of about 0.05 m thickness and an overlaying low shear layer of about 0.35 m thickness. We showed that these results are compatible with a Herschel–Bulkley or a Cross rheological model, but incompatible with a Bingham or Newtonian model. However, since there does not appear to be a well defined transition between the shear layer and the plug-flow this suggests that the Cross model is most appropriate.

Note, however, that flow normal velocity components have not been measured and therefore have not been considered in the analysis of the measurement results. This means that the obtained effective shear stress may also include Reynolds stresses due to flow normal velocity components.

From the velocity measurements, we estimated the energy dissipation in the basal layer and in the shear layer of our experimental flow. The estimated energy dissipation may explain the icy surfaces which are frequently observed in the tracks of flowing avalanches of moderate velocity (or considerable duration, respectively).

The main weakness of this work is that it is essentially based on only one experiment. To provide a rigorous test of the internal constitutive behaviour and the lower boundary condition, a large number of experiments need to be performed with identical snow. The flow depth, basal surface and slope inclination should all be varied. In addition, the vertical fluctuation velocities should also be measured to assess whether the flows are turbulent or laminar.

As the current velocity sensor layout does not provide the possibility to resolve flow normal velocity components, those could not be taken into account in the current analysis. Measurements of two-dimensional velocities in the shear layer of chute flows of snow will provide a more sophisticated understanding of the structure of the shear layer of snow flows and more robust statements on the constitutive behaviour of flowing snow.

Acknowledgements

This work has been part of the project "Numerical analysis and experimental validation of flowing avalanches with special consideration of avalanche deflecting and catching dams" funded by the Swiss National Fund under Grant Number 20-65126.01. The authors wish to thank the SLF staff for technical support under difficult conditions. JNM is funded by the Isaac Newton Trust and the EU SATSIE project. Helpful discussions with Christophe Ancey and Othmar Buser are gratefully acknowledged.

References

Ancey, C., Coussot, P., Evesque, P., 1996. Examination of the possibility of a fluid-mechanics treatment for dense granular flows. Mech. Cohes.-Frict. Mater. 1, 385–403.

Barnes, H.A., Hutton, J.F., Walters, K., 1989. An Introduction to Rheology Elsevier, Amsterdam.

Bartelt, P., Salm, B., Gruber, U., 1997. Modelling Dense-Snow Avalanche Flow as a Criminale-Ericksen-Filby Fluid without Cohesion. Internal Report 717, Swiss Federal Institute for Snow and Avalanche Research.

Dent, J., 1986. Flow properties of granular flows with large overburden loads. Acta Mech. 64, 111–122.

Dent, J.D., Lang, T.E., 1982. Experiments on the mechanics of flowing snow. Cold Reg. Sci. Technol. 5 (3), 253–258.

Dent, J., Lang, T., 1983. A biviscous modified Bingham model of snow avalanche motion. Ann. Glaciol. 4, 42–46.

Dent, J., Burrel, K., Schmidt, D., Louge, M., Adams, E., Jazbutis, T., 1997. Density, velocity and friction measurements in a dry snow avalanche. Ann. Glaciol., 26.

Gubler, H., 1986. Measurements and modelling of snow avalanche speeds. Proceedings of Avalanche Formation, Movements and Effects, vol. 162. IAHS Publication, pp. 405–420. Davos.

Hutter, K., Koch, T., 1991. Motion of a granular avalanche in an exponentially curved chute: experiments and theoretical predictions. Philos. Trans. R. Soc. Lond., A (334), 93–138.

Hwang, H., Hutter, K., 1995. A new kinetic model for rapid granular flow. Contin. Mech. Thermodyn. (7), 357–384.

Issler, D., 2003. Experimental information on snow avalanches. In: Hutter, K., Kirchner, N. (Eds.), Dynamic Response of granular and porous materials under large and catastrophic deformations, pp. 109–160.

Jenkins, J., Mancini, F., 1987. Balance laws and constitutive relations for plane flows of a dense, binary mixture of smooth, nearly elastic discs. J. Appl. Mech. 109, 27–34.

Koch, T., Greve, R., Hutter, K., 1994. Unconfined flow of granular avalanches along a partly curved surface, Part II. Proc. R. Soc. Lond., A (445), 415–435.

Louge, M., 1994. Computer simulations of rapid granular flow of spheres interacting with a flat, frictional boundary. Phys. Fluids 6 (7), 2253–2269.

Maeno, N., Nishimura, K., 1979. Fluidization of snow. Cold Reg. Sci. Technol. 1 (2), 109–120.

Maeno, N., Nishimura, K., Kaneda, Y., 1980. Viscosity and heat transfer in fluidized snow. J. Glaciol. 26 (94), 263–274.

Mannheimer, R.J., 1991. Laminar and turbulent flow of cement slurries in large diameter pipe: a comparison with laboratory viscometers. J. Rheol. 35 (1), 113–133.

McElwaine, J., Tiefenbacher, F., 2003. Calculating internal average velocities from correlation with error analysis. Surv. Geophys. 24, 499–524.

Metzner, A.B., Reed, J.C., 1955. Flow of non-Newtonian fluids—correlation of the laminar transition and turbulent-flow regions. AIChE J. 1, 434–440.

Nishimura, K., 1990. Studies on the fluidized snow dynamics. Contrib. Inst. Low Temp. Sci., Hokkaido Univ., Ser. A (37), 1–55.

Nishimura, K., Ito, Y., 1997. Velocity distribution in snow avalanches. J. Geophys. Res. 102 (B12), 27297–27303.

Nishimura, K., Maeno, N., 1986. Experiments on snow avalanche dynamics. Proceedings of Avalanche Formation, Movements and Effects, vol. 162. IAHS Publication, pp. 395–404. Davos.

Nishimura, K., Maeno, N., Sandersen, F., Kristensen, K., Norem, H., Lied, K., 1993. Observations of the dynamic structure of snow avalanches. Ann. Glaciol. 18, 313–316.

Norem, H., Irgens, F., Schieldrop, B., 1986. A continuum model for calculating snow avalanche velocities. Proceedings of Avalanche Formation, Movements and Effects, vol. 162. IAHS Publication, pp. 363–378. Davos.

Norem, H., Irgens, F., Schieldrop, B., 1989. Simulation of snow avalanche flow in runout zones. Ann. Glaciol. 13, 218–225.

Oldroyd, J.G., 1947. A rational formulation of the equation of plastic flow for a Bingham solid. Proc. Camb. Philos. Soc. 43, 100–105.

Savage, S., Hutter, K., 1991. The dynamics of granular materials from initiation to runout: Part I. Analysis. Acta Mech. 86, 201–231.

Tiefenbacher, F., Kern, M., 2004. Experimental devices to determine snow avalanche basal friction and velocity profiles. Cold Reg. Sci. Technol. 38, 17–30.